한국표면공학회지
Journal of the Korean Institute of Surface Engineering
Vol. 26, No. 3, June 1993
<연구논문>

Voltammetric Study on the Underpotential Deposition of Zinc

Joong Bae Lee
Korea Academy of Industrial Technology, 472 Gajwa 4-dong, Seo-gu, Incheon, Korea
Paul F. Duby
Henry Krumb School of Mines, Columbia University
New York, N. Y. 10027, USA

초 록

탄소강 및 Nickel 음극에서 아연의 전착특성에 대하여 조사하였다. 황산아연 및 염화아연용액속에서 회전전극을 사용하여 실험한 결과 아연의 평형전위 이전에서 전착이 일어나는 소위 Underpotential Deposition 현상이 관찰되었다. 또한 이렇게 전착이 일어난 아연층은 평형상태에서 일정한 두께로 제한되는데 전착전압에 따른 전착층의 전하량을 계산한 결과 다층흡착구조과 유사한 경향을 나타내었다.

1. INTRODUCTION

Galvanization is widely used to protect iron and steel from atmospheric corrosion. Recently, zinc has been alloyed with iron-group metals because of the superior properties of these alloys such as corrosion resistance, weldability, and also paintability[1]. The electrodeposition of zinc with iron-group metals is called anomalous codeposition; it yields anomalously high zinc content in the codeposited alloys. Nicol and Philip[2] have attempted to relate such anomalous behavior with the phenomenon of underpotential deposition. Swathirajan[3] investigated the inhibiting effect of underpotentially deposited zinc on the electrodeposition of nickel.

The underpotential deposition of monolayer of a metal on a foreign substrate has been studied for various metal-substrate systems[2-9], and a general relationship was proposed by Kolb et al.[6]

$$\triangle U_d = \frac{\Delta\Phi}{2} \quad (1)$$

where $\triangle U_d$ is the shift of electrodeposition potential in V, and $\Delta\Phi$ is the difference of work function values between the substrate and the electrodeposited metal in eV. Quantitative studies, however, have been limited to a few cases such as copper on noble metals[4,7,8]. The underpotential deposition of zinc on different substrates has been mentioned in several papers[2,7,9]. A major difficulty for the study of zinc is the simultaneous evolution of hydrogen.

In this report, the underpotential deposition of zinc was investigated on carbon steel substrate both in sulfate and chloride solution, and

also on electroplated nickel.

2. EXPERIMENTAL

A rotating disk system with the working electrode in a Teflon insulator was used in a 0.5 l glass cell. The material was 1018 carbon steel with a chemical composition of 0.15−0.20% C, 0.6−0.9% Mn, 0.04% Max P, and 0.05% Max S. The exposed geometric area was 0.46cm². This carbon steel was used as substrate for most experiments. Another substrate, a bright nickel surface was prepared by electroplating in 0.5 M nickel sulfate solution at 300 mA/cm². Before each measurement, the electrode was polished with fine alumina powder (0.05μ) to a mirror-like surface, and cleaned first with acetone and then activated with dilute sulfuric acid. A saturated calomel electrode was the reference electrode, and a platinum wire was the counter electrode.

Solutions were 0.5 M zinc sulfate or zinc chloride prepared with reagent grade chemicals. The pH was adjusted to 3.0 with sulfuric acid or hydrochloric acid. The only impurity detected by inductively coupled plasma (ICP) spectrometer was iron at the level of about 0.05 ppm. The solution was purified by electrolysis at a constant potential −0.9 V (vs. SCE) with a platinum rotating disk electrode. It was sparged with purified nitrogen to remove the dissolved oxygen just before the measurements.

The polarization curves were obtained by linear sweep voltammetry at a sweep rate of 100 mV/sec. For the electrodeposition, the potential was driven in the negative direction, then reversed. For stripping tests, the potential was held at a given value, then driven in the positive direction. In some cases, the current transients were recorded as a function of time by means of a storage oscilloscope. The ohmic drop in the solution was determined by the current interruption method, and a correction was applied to each polarization curve.

3. RESULTS

Fig. 1 represents a linear sweep voltammetry obtained with the carbon steel electrode in a zinc sulfate solution. During the cathodic sweep, a small peak is observed at about −0.93 V (vs. SCE). The current starts to increase again at −1.03 V which is the normal electrodeposition potential of zinc. A shoulder is observed at the beginning of this steady rise, as the surface becomes covered by zinc. The anodic sweeps intersects the zero current line at −1.05 V.

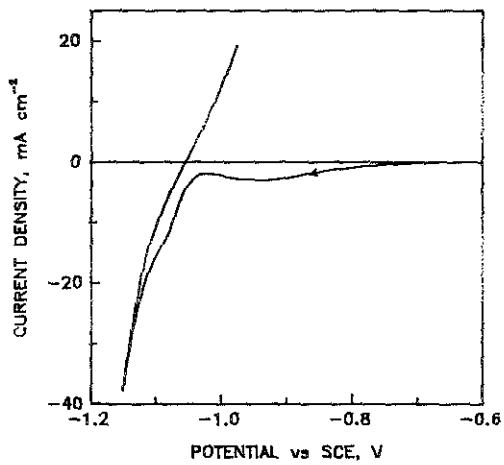

Fig. 1. Linear sweep voltammetry on carbon steel (0.5 M $ZnSO_4$, pH 3.0, temperature 25 ℃, rotating speed 2500 rpm, sweep rate 100 mV/sec).

The result was also compared with an interrupted sweep illustrated by curve 1 in Fig. 2. The potential was held at the peak −0.93 V for 5 seconds, then the sweep was resumed. During this short period of time, the current rapidly decreases. Curve 2 in Fig. 2 shows the potential sweep in the absence of zinc in the solution. Hydrogen evolution begins at about −0.7 V, and the current increases faster than in the presence of zinc (curve 1), although later it becomes limited by diffusion.

The current transients were obtained at four potentials as illustrated in Fig. 3. The potential steps were applied after keeping the electrode

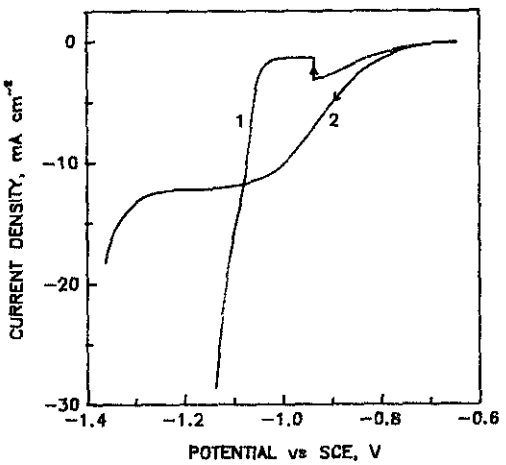

Fig. 2. Linear sweep voltammetry on carbon steel in 0.5M $ZnSO_4$ (curve 1) and in 0.5 M $Na2SO_4$ without $ZnSO_4$ (curve 2) (pH 3.0, temperature 25℃, rotating speed 2500 rpm, sweep rate 100 mV/sec).

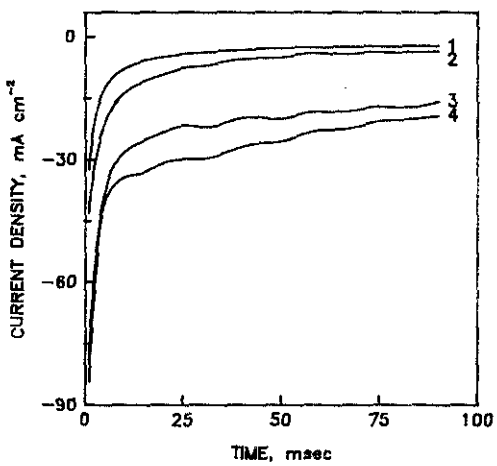

Fig. 3. Potentiostatic current transients on carbon steel at four different potentials, 1: −1.000 V (vs. SCE), 2: −1.050 V, 3: −1.100 V, 4: −1.150 V (0.5 M $ZnSO_4$, pH 3.0, temperature 25℃, rotating speed 2500 rpm).

at the rest potential for about 20 seconds. All four curves show rapid current decreases. At a potential of −1.000 V, for instance, the current decreases to about 2 mA/cm² in 0.1 second, and then more slowly to a steady-state current of 0.75 mA/cm² in 10 seconds. At −1.050 V, the steady-state current is also very low, while at the potential of −1.100 V and −1.150 V which are more negative than the reversible potential of zinc, the steady-state currents are much higher than the first two.

Fig. 4 shows another current transient obtained at a more negative potential, −1.250 V and with a longer time scale. It initially has a similar shape to the four curves in Fig. 3, but the current begins to increase after 0.3 second as the electrodeposition continues. The dashed line displays an example of rapid current increase for the three-dimensional growth of nickel layer on carbon steel.

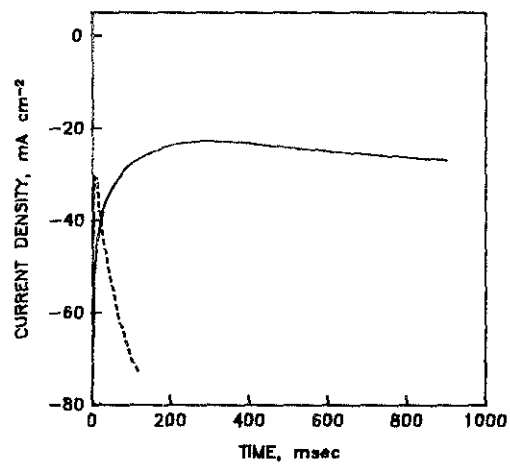

Fig. 4. Potentiostatic current transients on carbon steel in 0.5 M $ZnSO_4$ at −1.250 V (solid line) and in 0.5 M $NiSO_4$ at −1.1 V (dashed line) (pH 3.0, temperature 25 ℃, rotating speed 2500 rpm).

Fig. 5 shows the steady-state polarization curves obtained by the potential step method in a sodium sulfate solution (curve 1), and in a zinc sulfate solution (curve 2). The steady-state current at about −0.85 V is almost the same for both cases. As the potential becomes more negative, however, current becomes much smaller.

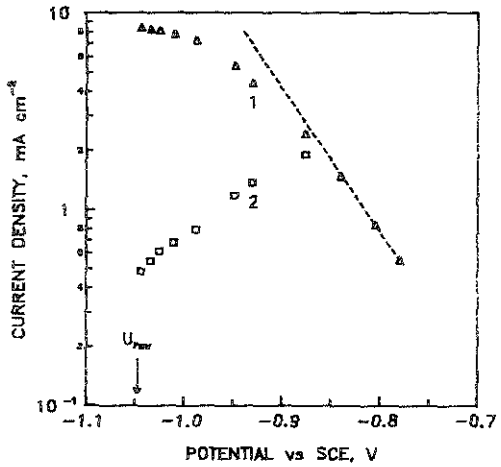

Fig. 5. Steady-state currents on carbon steel at different overpotentials in 0.5 M Na_2SO_4 (curve 1) and in 0.5 M $ZnSO_4$ (curve 2) (pH 3.0, temperature 25℃, rotating speed 2500 rpm). Dashed line represents Tafel line.

Fig. 6 illustrates the effect of reversing the sweep at two different potentials. Curve 1 was reversed at −1.06 V, and curve 2 was reversed at −1.02 V. The difference in the shape of the anodic branches was attributed to the stripping of a different amount of zinc electrodeposited during the two cathodic sweeps.

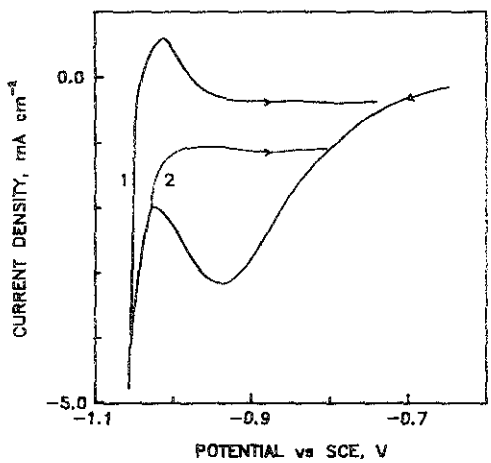

Fig. 6. Cyclic sweep voltammetry on carbon steel reversed at two different potentials, 1: −1.06 V (vs. SCE), 2: −1.02 V (0.5 M $ZnSO_4$, pH 3.0, temperature 25℃, rotating speed 2500 rpm, sweep rate 100 mV/sec).

Fig. 7 illustrates the anodic sweeps obtained after maintaining the electrode potential at preset values for 10 seconds. All curves display anodic shoulders and/or the peaks at −0.85 V (B) and −0.99 V (A), which represent the stripping of zinc layers formed in the underpotential range. For electrodeposition times longer than 10 seconds, the anodic curves were reproducible. The amount of charge passed during anodic stripping was calculated by the areas under the shoulders and peaks as illustrated by curve 4 in Fig. 7. The dashed line was obtained by cubic spline fitting of solid line data at starting point and after the peak. Similar technique has been used by Breiter[4].

The relationship between the electrodeposition potential and the corresponding amount of charge is shown in Fig. 8. Three curves repres

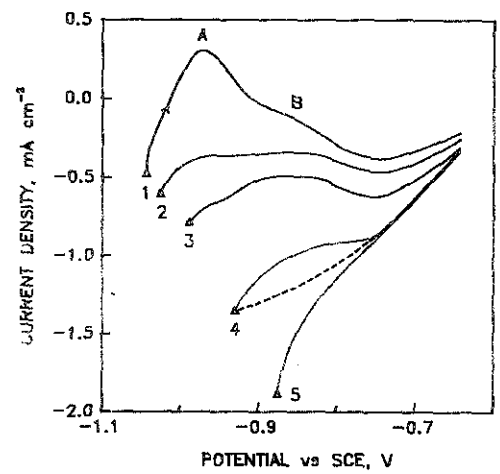

Fig. 7. Linear potential sweeps in anodic direction after holding potential for 10 sec at five different values, 1: −1.044 V (vs. SCE), 2: −1.025 V, 3: −0.988 V, 4: −0.930 V, 5: −0.876 V (0.5 M $ZnSO_4$, pH 3.0, temperature 25℃, rotating speed 2500 rpm, sweep rate 100 mV/sec).

ent respectively the results obtained on carbon steel in sulfate and chloride solution, and also on electroplated nickel in sulfate solution. The data points in Fig. 8 were the average values obtained after the repetition of tests under different conditions. In Fig. 7, for instance, curve 4 was obtained at a sweep rate of 100 mV/sec after electrodeposition at −0.93 V for 10 seconds. The procedure was then repeated several times at different sweep rate: 20 mV/sec, 50 mV/sec, 100 mV/sec, and for different electrodeposition time: 10 seconds, 20 seconds, 30 seconds. Each test was done on the newly prepared electrode surface. The average value of estimated charge density was 0.214 mC/cm² (standard deviation 0.007). All three curves have a similar shape with the amount of charge increasing when the potential becomes more negative. The measured charge is higher in chloride solution than in sulfate solution (curve 2 vs. 1), and the reduction starts at a less negative potential on nickel than on carbon steel (curve 3 vs. 1).

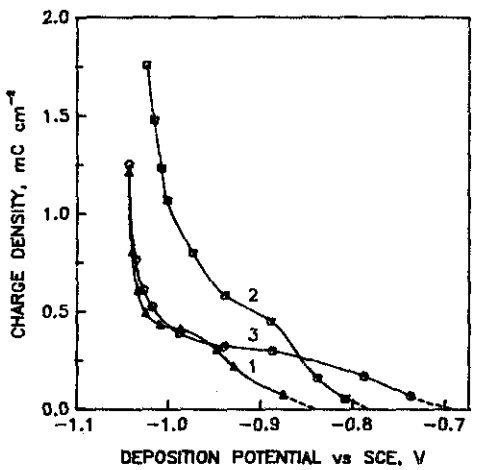

Fig. 8. Calculated charge densities of reduced zinc as a function of electrodeposition potential in 0.5 M $ZnSO_4$ (curve 1) and 0.5 M $ZnCl_2$ (curve 2) on carbon steel, and in 0.5 M $ZnSO_4$ on electroplated nickel (curve 3) (pH 3.0, temperature 25°C , rotating speed 2500 rpm, sweep rate 100 mV/sec).

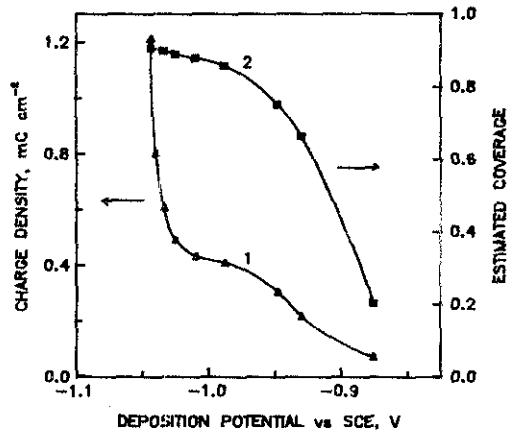

Fig. 9. Surface coverage estimated by ratio of hydrogen evolution currents in 0.5 M $ZnSO_4$ (curve 1) and in 0.5 M Na_2SO_4 (curve 2) (pH 3.0, temperature 25°C, rotating speed 2500 rpm).

4. DISCUSSION

The experimental results presented in Fig. 2 indicate that the hydrogen evolution is significantly suppressed in the presence of zinc. It is also observed from the anodic stripping curves of Fig. 7 that the cathodic surface is covered by a layer of reduced species in a potential range more positive than the reversible potential of zinc. All results can be interpreted by the underpotential deposition of zinc.

In Fig. 1, the intercept with the zero current line represents the point where the small rate of zinc corrosion equals the rate of hydrogen evolution. The hydrogen evolution current on zinc is quite small as shown in Fig. 5, and then it affects to the determination of reversible potential of zinc less than 2 mV, considering the steepness of anodic sweep curve. Therefore, the potential −1.05 V at the intercept is almost in agreement with the reversible potential of zinc, −1.048 V, calculated from the standard electrode potential and the activity coefficient data given by Latimer[10].

The cathodic peak in Fig. 1 is attributed to

the competition between the hydrogen evolution and the underpotential deposition of zinc; the current rises at about −0.70 V as the hydrogen evolution begins, but the process is partly suppressed as the surface becomes covered by a zinc layer, product of the underpotential deposition. The suppression of hydrogen evolution is expected given the high value of overpotential on a zinc surface.

The current vs. time curves in Fig. 3 are consistent with the change of cathodic surface as a function of time. Both curve 1 and 2 were obtained at less negative potentials than that for the electrodeposition of bulk zinc. The decrease of current corresponds to the build-up of a zinc layer (either a monolayer or a multilayer) which is two-dimensionally limited. The steady-state current, −0.45 mA/cm² for curve 1 and −0.75 mA/cm² for curve 2, attained in 10 seconds represents the hydrogen evolution current after the surface is covered by a zinc layer. The potential values for curve 3 and 4 are negative enough for the electrodeposition of zinc. The currents at these two potentials represent the currents for zinc electrodeposition and simultaneous hydrogen evolution. The gap in the current value between curve 2 and 3 is considered as a change from the underpotential deposition to the bulk layer electrodeposition. However, curve 3 and 4 do not have the shapes of three−dimensional crystallization in this time range. Fig. 4 indicates that the three-dimensional growth begins after the carbon steel substrate is covered by zinc, after the effect of original substrate is disappeared.

All three curves in Fig. 8 display the features of an isotherm for a multilayer adsorption process. A similar shape of curve has been obtained for the underpotential deposition of copper on palladium by Chierchie and Mayer[8]. Each curve features a knee which indicates the monolayer adsorption. The position of the knee is related to the electrodeposition potential at the completion of a zinc monolayer before it grows to a multilayer. It can be also related to the anodic stripping results in Fig. 7. At least, the curves show peak B until the electrodeposition potential becomes more negative than a value corresponding with the position of the knee. Therefore, peak B alone corresponds to the electrodeposition of a zinc monolayer. Considering the theoretical amount of charge for a monolayer, 0.52 mC/cm² on the basal plane of hexagonal-closed-packed crystal, the zinc layer corresponding to peak B will be a fraction of monolayer. On the other hand, the amount of charge for peak A and B is much higher than that for a monolayer. The peak A corresponds to the electrodeposition of a multilayer which probably commences just before the deposition of bulk layer. The presence of this layer has been mentioned in some other papers[4)6)8)].

In the underpotential range, the surface coverage of zinc increases as the potential becomes more negative. Fig. 5 shows that the hydrogen evolution is suppressed at higher coverage of zinc. For instance, the steady-state current at −1.044 V is about −0.48 mA/cm² which is much smaller than that on bare carbon steel, −8.26 mA/cm². At this potential, the substrate is expected to be almost completely covered by zinc, and the steady-state current represents only the hydrogen evolution on zinc. By drawing the imaginary Tafel line crossing this point, the exchange current density for the hydrogen evolution on zinc is estimated to be at least two orders of magnitude smaller than that on carbon steel. The rate of hydrogen evolution on the partial zinc layer compared to that on the bare carbon steel substrate can be neglected. Therefore, the steady-state coverage of zinc at a given potential can be roughly estimated from the ratio of two hydrogen evolution currents in the solutions with and without zinc as illustrated in Fig. 9. The coverage increases with the corresponding amount of charge, resulting in a

plateau as it becomes completed. The position of the knee almost agrees with that of curve 1 which represents the completion of monolayer, as discussed above.

The reported work function of zinc is 4.33 eV[11], and that for polycrystalline α-iron is 4.70 eV[12]. Assuming that the work function of low carbon steel is the same as that of pure iron, the electrodeposition potential of zinc on carbon steel is to be shifted by 0.185 V according to Eq. 1. The underpotential deposition of zinc is then expected at −0.865 V. The work function of nickel is 5.15 eV13), and the underpotential deposition of zinc is expected at −0.64 V. The values of potential for the underpotential deposition of zinc can be estimated either by the intercept of two curves in Fig. 5 or by extrapolating the curves in Fig. 8 to zero charge. The values estimated in two different figures are in agreement (−0.86 V vs. −0.84 V). The values are listed in Table 1.

Table 1. Potentials for Underpotential Deposition

Condition	by Eq. 1 V (vs. SCE)	by Experiment
Steel in Sulfate	−0.865	−0.85
Steel in Chloride	−0.865	−0.79
Nickel in Sulfate	−0.640	−0.69

The potential values obtained for under-potential deposition on carbon steel in sulfate solution agrees fairly well with that expected from Eq. 1, whereas the value obtained in chloride solution is more positive. The specific adsorption of chloride ions may change the property of original surface. Kolb et al. have mentioned that the chloride solution causes a shift of underpotential deposition to a more negative potential than in a sulfate solution[6]. Our results do not confirm that statement. For underpotential electrodeposition on the electroplated nickel, the value is slightly negative than predicted by Eq. 1, but it is still in fair agreement.

5. CONCLUSION

Zinc can be electrodeposited on carbon steel and electroplated nickel in the underpotential range. The result in sulfate solution agrees with the equation proposed by Kolb et al., but the potential in chloride solution is shifted in the positive direction.

The coverage of the carbon steel substrate by zinc in sulfate and chloride solutions as well as the coverage of nickel by zinc in sulfate solution can be described from experimental result. This suggests that the surface coverage corresponds to a thermodynamic equilibrium controlled by the cathodic potential. The shape of curves in Fig. 8 warrants further analysis using multilayer adsorption model. The results will be presented in the following paper.

ACKNOWLEDGMENT

This research has been supported by the U. S. Department of the Interior's Mineral Institutes Program administered by the Bureau of Mines under allotment grant # G1194136.

REFERENCES

1. R. Noumi, H. Nagasaki, Y. Foboh, and A. Shibuya : SAE Technical Paper, 820332 (1982)
2. M. J. Nicol and H. I. Philip : J. Electroanal. Chem., 70 (1976) 233
3. S. Swathirajan : J. Electroanal. Chem., 221 (1987) 211
4. M. W. Breiter : J. Electrochem Soc., 114 (1967) 1125
5. D. J. Astley, J. A. Harrison, and H. R. Thirsk : J. Electroanal. Chem., 19 (1968) 325
6. D. M. Kolb, M. Przasnyski and H. Gerischer : J. Electroanal. Chem., 54 (1974) 25
7. D. M. Kolb and H. Gerischer : Surface Sci., 51 (1975) 323
8. T. Chierchie and C. Mayer : Electrochim.

Acta, 33 (1988) 341
9. T. J. O'Keefe and M. W. Mateer : Physical Chemistry of Extractive Metallurgy, Ed. V. V. Kudryk and Y. K. Rao, TMS of AIME, New York, (1985) 165
10. W. M. Latimer : The Oxidation States of Elements and Their Potentials in Aqueous Solutions, Ed. W. M. Latimer, Prentice Hall, New Jersey, (1952) 354
11. R. Suhrmann and G. Wedler : Z. Angew. Phys., 14 (1965) 70
12. A. Gardwell : Phys. Rev., 92 (1953) 554
13. D. E. Eastman : Phys. Rev. Sect. B, 2 (1970)